Abstract

A finite element model is used to simulate a push-pull ventilation system in three spatial dimensions. The turbulent Navier-Stokes equations and the turbulence kinetic energy equation are solved employing a one equation turbulence model. A test case is a simple push-pull system consisting of a square jet and square hood. Velocity and turbulence fields are calculated for the test case with cross draft velocities of 0, 100, and 250 fpm. Measurements of velocity and turbulence fields were performed to validate the numerical predictions using a visualization technique and hot-film anemometry. Velocity field predictions were reasonable, however, turbulence predictions were not as good. The discrepancy is probably due to an inadequate turbulence model and numerical errors resulting from calculations on coarse grids.

Acknowledgments

Thank you God.

I would like to appreciate Mike Flynn for his guidance in my study. Nothing could have been accomplished without his help. Special thanks to Maryanne Boundy, Taehyeung Kim, and David Leith for their precious help and encouragement. Thank Dr. Cass Miller for allowing me to see his world of profound knowledge. I am gratitude to Carol Carden, Gary Carlton, Steve Cooper, C L Lassiter, Dr. Katherine Murphy, G. Ramachandran, Pete Raynor, and Dr. Lori Todd for their kindness.

Thank my family for their support and dedicate this little piece to my late father who gave me everything except my opportunity for rewarding.

Table of Contents

List of Tables

List of Figures

Abbreviations

CI	Confidence Interval
FDM	Finite Difference Method
FEM	Finite Element Method
LEV	Local Exhaust Ventilation
LUD	Lower-Upper Decomposition
TKE	Turbulence Kinetic Energy
TSI	Thermo System Inc.
cfh	cubic feet per hour
cfm	cubic feet per minute
fpm	foot per minute
ft	foot/feet
in	inch/inches
lb	pound/pounds

Notation

A_2	turbulence model constant (0.5)
C	concentration
C_2	turbulence model constant (0.18)
D	mass diffusivity
D_j	jet diameter
D_t	eddy diffusivity
F	frequency of inverter
I	intercept of regression line
P	dynamic pressure
Q	calibration flow (cfm)
R	rotometer reading (cfh)
S	slope of regression line
U_c	cross draft velocity
V	wind tunnel velocity (fpm)
Vel	velocity normal to the sensor (fpm)
$Volt\ 1$	#1 sensor bridge voltage (volts)
$Volt\ 2$	#2 sensor bridge voltage (volts)
W	wet test meter reading (cfh)
X	measured value
Y	predicted value
$"H_2O$	inches of water column
h	orifice meter pressure drop ($"H_2O$)
i	component of the solution vector
k	kinetic energy of turbulence
m	iteration level.

r	variable
$\bar{u}$	velocity vector
u	x component of velocity vector
v	y component of velocity vector
w	z component of velocity vector
w_{ex}	velocity at hood face
x	distance from the origin in x direction
y	distance from the origin in y direction
z	distance from the origin in z direction
Λ	length scale
α	error criterion
ε	dissipation rate of turbulence kinetic energy
γ_p	penalty parameter
λ	distance measured normal from the nearest wall
μ	dynamic viscosity of air
σ_t	Prandtl number.
ρ	density of air
τ_w	shear stress
ν	laminar kinematic viscosity
ν_e	effective kinematic viscosity
ν_t	eddy kinematic viscosity

Introduction

Local exhaust ventilation (LEV) systems are widely used to capture and remove emissions from industrial processes. The local exhaust hood is placed close to the emission source to create an air flow field that effectively controls contaminants and prevents worker exposure. However, a disadvantage of the LEV is the rapid decrease in velocity with distance from the hood[1]. In addition, the flow field may be disrupted by general ambient air, make-up air flow, cooling fans, and movement of personnel[2]. Also, there are some cases, such as a wide surface tank, where the placement of the hood to control the whole emission area is very difficult.

In this situation, a push-pull ventilation system, consisting of a push nozzle and an exhaust hood, has been used effectively to eliminate contaminated air above the tank. The push jet flow carries the pollutants and the pull flow accepts and removes the push jet flow. Since the velocity of the jet flow decays much less rapidly with distance than that of the hood flow, the push jet controls the polluted air better. Furthermore, operating costs are reduced because a well-designed push-pull ventilation system uses smaller volumes of exhaust air than typical local exhaust alone to achieve the same efficiency of contaminant control. For these reasons, push-pull ventilation has been applied to open surface tanks, air curtain, and other industrial applications[3] and specific design criteria have been developed experimentally for some open surface vessels and other processes[1,3]. However, these design criteria are applicable only to the originally tested set-ups. They do not provide enough information to predict the flow field and contaminant concentration at points where workers breathe.

Numerical modeling, through the application of computational fluid dynamics techniques, is an important means in the design process for ventilation. Numerical study has less restrictions than experimental study and has the potential of providing information that can not be obtained by experiments.

A few studies have reported numerical modeling of the push-pull ventilation. Heinsohn et al.[4] presented numerical solutions of flow over an open vessel controlled by a push-pull system. Lage et al.[5] studied a slot ventilated enclosure with one inlet and one outlet. Both studies used two-dimensional finite difference method (FDM), the SIMPLE algorithm[6], and the k-ε turbulence model[7]. Damin et al.[8] used two-dimensional FDM with a one-equation turbulence model. Only one study[9] presented three-dimensional calculations of room air distribution with inflow and outflow boundary conditions. All these studies lacked suitable quantitative experimental validation. A three-dimensional finite element method (FEM) code has been developed by Flynn[10] to solve the turbulent Navier-Stokes equations. This code predicts the velocity and turbulent kinetic energy fields resulting from a push-pull ventilation system with cross draft.

The purpose of this study is to improve the design of the push-pull ventilation systems by applying numerical simulations. Predictions from numerical simulations can supply the information on velocity and concentration fields that are needed in the design process. Concentration fields can be predicted when velocity and turbulent fields are known.

The objectives of this work are (i) to predict the velocity and turbulence fields of push-pull flows by applying the three-dimensional finite element code and (ii) to validate the predictions by comparing them to experimental measurements. The specific case examined here is a coaxial square jet and square hood with cross flow perpendicular to the coaxial centerline of the jet and hood. The air flow of the system is assumed incompressible, steady, and iso-thermal.

2

Theory

The push-pull flow field is very complex. It is time-dependent, non-linear and three-dimensional and has both viscous and turbulent properties. However, we are generally interested in finding only gross flow characteristics, such as time-averaged velocity and concentration. The mathematical model for the flow consists of the continuity equation, Navier-Stokes equations (momentum equations), and turbulence model.

Governing Equations

The governing equations are listed below. All variables are time-averaged values.

- Incompressible Continuity (conservation of mass)

$$\nabla \cdot \bar{u} = 0 \tag{1}$$

where $\bar{u}$ is the velocity vector.

- Navier-Stokes (conservation of linear momentum)

$$\bar{u} \cdot \nabla \bar{u} + \nabla P - \nabla \cdot \left[\left(\nu_e (\nabla \bar{u} + \nabla \bar{u}^T) \right) \right] = 0 \tag{2}$$

where P is the dynamic pressure, and ν_e is the effective kinematic viscosity, which is the sum of the laminar kinematic viscosity (ν) and the eddy kinematic viscosity (ν_t)

$$\nu_e \equiv \nu + \nu_t \tag{3}$$

The eddy viscosity is defined by the Kolmogorov-Prandtl approximation:

$$\nu_t = C_2 \Lambda k^{1/2} \tag{4}$$

where C_2 is a constant ($0.18^{[10]}$), Λ is a length scale, and k is the kinetic energy of turbulence.

A simple length scale expression[11] is used:

$$\Lambda = 0.25 D_j + 0.025(x^2 + y^2 + z^2)^{1/2} \tag{5}$$

3

where D_j is the jet diameter, which is approximated by the width of a square jet of equivalent face area, and x, y, z are the distance from the origin in x, y, and z direction. The origin is located at the center of jet face.

- Turbulence Kinetic Energy

$$\bar{u} \cdot \nabla k = v_t \left[\nabla \bar{u} \cdot (\nabla \bar{u} + \nabla \bar{u}^T) \right] + \nabla \cdot (v_t \nabla k) - A_2 \frac{k^{3/2}}{\Lambda} + v \nabla^2 k \qquad (6)$$

where A_2 is a constant (0.5[10]).

- Advective-Diffusive Equation

$$\bar{u} \cdot \nabla C = \nabla \cdot \left[(D + D_t) \nabla C \right] \qquad (7)$$

where C is concentration, D is the mass diffusivity, D_t is the eddy diffusivity ($D_t = \frac{v_t}{\sigma_t}$) and σ_t is the Prandtl number.

Concentration predictions depend upon velocity and a turbulent diffusion coefficient, which is calculated locally by the relationship $\Gamma = \frac{v_L}{\sigma_t}$. The Prandtl number is an empirical constant. The eddy viscosity is proportional to the product of the turbulence kinetic energy and the length scale. Thus, concentration predictions are related to the turbulence and velocity characteristics.

Turbulence Model

A turbulence model is needed to close the time-averaged momentum equations. The two-equation k-ε model[7] has been most widely used in turbulent flow calculations, but an additional equation for the dissipation rate of turbulence kinetic energy (ε) must be solved. Even though the k-ε model is known to be more general and robust for turbulence problems, it increases the size of the problem and computational efforts. Sykes et al.[11] proposed a one-equation model with a geometric length scale expression, which was

4

empirically determined to fit a straight jet and then applied successfully to a jet in a perpendicular cross draft.

Numerical Methods

The main features of the solution procedure are the Bubnov-Galerkin finite element method[12], a under-relaxation substitution method[13], the lower-upper decomposition (LUD) method[13], the penalty function method[14,15], a simple upwinding scheme[16], the one-equation turbulence model[11], and the wall function method[17,18].

Finite Element Model Calculations

Figure 1 depicts the computational domains. Due to symmetry, only one quadrant or one-half the flow field was modeled. A Cartesian coordinate system was adopted with its origin located at the center of the square jet. The physical system was subdivided into a series of rectangular brick elements. For formulation, the code used the Bubnob-Galerkin weighted residual method which employed a tri-linear basis function and assumed the weighting function was equal to the basis function. A banded storage scheme was used to reduce storage requirement and the LUD method was applied to solve the assembled global matrix equations. The successive under-relaxation substitution was used in order to handle the non-linear problem. The relaxation factor was set to 0.5. An error criterion, α, is defined as the relative change in the solution vector from one iteration to next:

$$\alpha = \left[\frac{\sum_i \left(r_i^m - r_i^{m+1} \right)^2}{\sum_i \left(r_i^m \right)^2} \right]^{1/2} \tag{8}$$

where r is the variable, i is a component of the solution vector, and m denotes the iteration level.

The Bubnov-Galerkin FEM can cause spurious oscillations or non-convergence in convection-dominated turbulent flows such as a push-pull flow. Although severe mesh refinements can resolve this problem, this would be impractical for three-dimensional
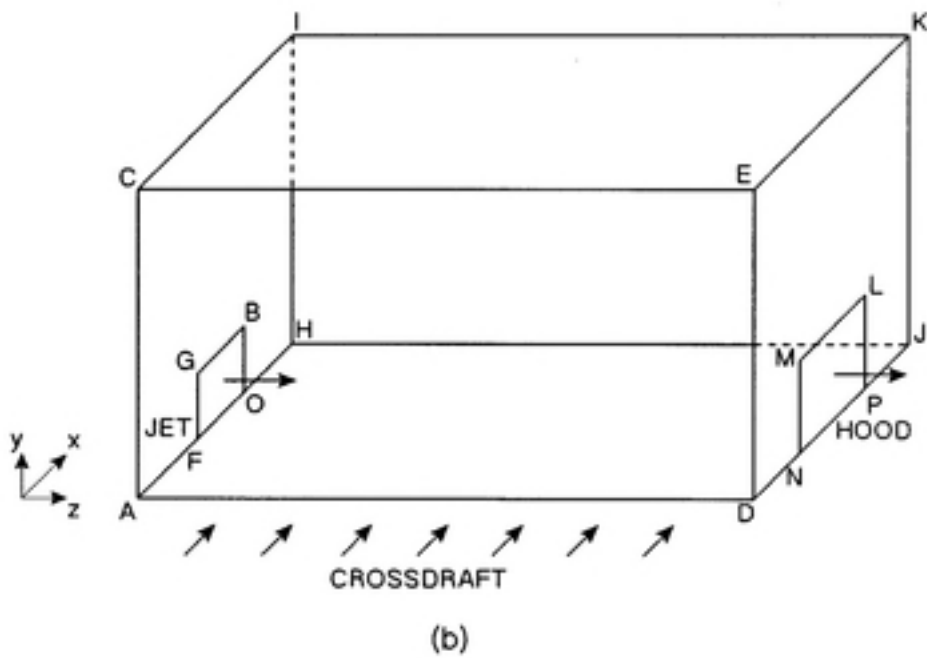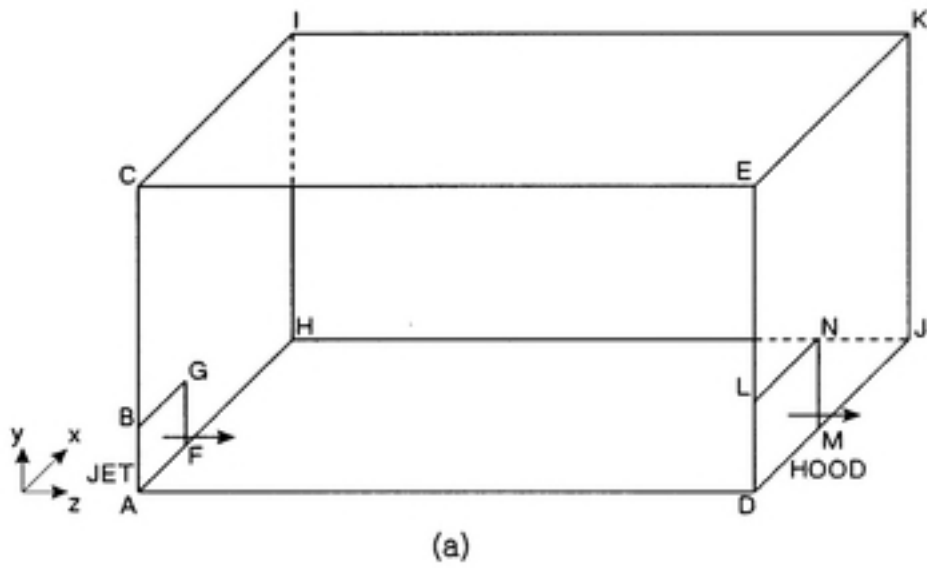
6

Figure 1. Computational Domains (a) The Square Jet and Square Hood without Cross Draft (b) The Square Jet and Square Hood with Cross Draft

calculations because huge number of grid points is required to produce right solutions. Therefore, to achieve upwinding, this code adopted a simple reduced quadrature scheme developed by Hughes[16].

Penalty Function Method

The penalty function method[14,15] allows elimination of pressure from the incompressible Navier-Stokes equations. The method effectively equates pressure to the negative of a penalty parameter multiplied by the continuity equation:

$$P = -\gamma_p (\nabla \cdot \bar{u}) \tag{9}$$

where γ_p is the penalty parameter.

This expression is then substituted into the Navier-Stokes equations. A proper value of penalty parameter is used to enforce continuity, which is set to $10^{7[14]}$.

Boundary Conditions

The boundary conditions are set as follows:

- A Square Jet - Square Hood without Cross Draft

    Jet face (AFGB)

    $$u = v = 0, w = 1, \text{ and } k = 0.001 \tag{10}$$

    where u, v, and w are the x, y, z component of velocity vector respectively.

    Hood face (DMNL)

    $$u = v = 0, w = w_{ex}, \text{ and normal derivative of } k \text{ is zero.} \tag{11}$$

    where is w_{ex} the velocity at the hood face.

    Walls (BGFHIC and MJKELN)

    $$w = 0, u, v, \text{ and } k \text{ are values assigned using the wall function approach.} \tag{12}$$

8

Symmetry planes (ADEC and ADJH)

ADEC $u = 0$, normal derivatives of v, w, and k are zeros. $\hfill (13)$

ADJH $v = 0$, normal derivatives of u, w, and k are zeros. $\hfill (14)$

Free surface planes (CEKI and HJKI)

$\quad w = 0$, normal derivatives of u, v, and k are zeros. $\hfill (15)$

Jet core (on the centerline of the jet and hood)

$$u = v = 0, \; w = 1, \text{ and } k = [0.00137 \, z \, / \, (C_2 \, \Lambda)]^2 \hfill (16)$$

- A Square Jet - Square Hood with Cross Draft

Jet face (FOGB)

$$u = v = 0, \; w = 1, \text{ and } k = 0.001 \hfill (17)$$

Hood face (NPLM)

$$u = v = 0, \; w = w_{ex}, \text{ and normal derivative of } k \text{ is zero.} \hfill (18)$$

Walls (AFGBLHIC and DNMLPJKE)

$\quad w = 0$, u, v, and k are values assigned using the wall function approach.

$$\hfill (19)$$

Inflow (ADEC)

$u = U_c$ + (flow through the plane NPLM)/(area of the plane ADEC),

$v = w = 0$, and normal derivative of k is zero. $\hfill (20)$

where U_c is the velocity of the cross draft.

Outflow (HJKI)

$u = U_c$, $v = w = 0$, and normal derivative of k is zero. $\hfill (21)$

Lateral (ADJH and CEKI)

ADJH $v = 0$, normal derivatives of u, w, and k are zeros. $\hfill (22)$

CEKI normal derivatives of u, v, w, and k are zeros. $\hfill (23)$

Jet core (on the centerline of the jet and hood)

$$u = v = 0, \; w = 1, \text{ and } k = [0.00137 \, z \, / \, (C_2 \, \Lambda)]^2 \hfill (24)$$

9

The standard k-ε model was devised for high Reynolds number turbulent flows. Close to solid walls, viscous effects predominate over turbulent ones so that the standard turbulence model cannot be applied there. Thus wall function methods or low Reynolds number formulations have been used with this model.

Low Reynolds number formulations enforce no-slip boundary conditions on walls and implement the equations right up to walls. Since these methods need many nodes and demand much computer memory and time, they are impractical for three-dimensional flow problems[19]. When using wall function methods, the first computational nodes are placed in a region some distance off the wall. The solution at the nodes is matched to values using wall functions. Launder and Spalding[7] presented a review of wall function methods.

A wall function approach[17,18] was used for these simulations. The calculation domain starts at distance of 1.0 S from the wall boundaries, where S is the half width of the jet. The following universal laws are valid in the near wall region[17,18].

$$u_i^* = \lambda^* \qquad\qquad 0 \le \lambda^* \le 5 \qquad (25)$$

$$u_i^* = \left(-3.05 + 5.0\log \lambda^*\right)\left(\frac{\tau_w}{|\tau_w|}\right) \qquad 5 \le \lambda^* \le 30 \qquad (26)$$

$$u_i^* = \left(-5.5 + 2.5\log \lambda^*\right)\left(\frac{\tau_w}{|\tau_w|}\right) \qquad \lambda^* \rangle 30 \qquad (27)$$

where

$$u_i^* = u_i \Big/ \sqrt{\left|\frac{\tau_w}{\rho}\right|} \qquad\qquad (28)$$

$$\lambda^* = \left(\frac{\lambda}{\nu}\right)\sqrt{\left|\frac{\tau_w}{\rho}\right|} \qquad\qquad (29)$$

i is 1 for boundaries parallel to the x-axis, 2 for boundaries parallel to the y-axis, 3 for boundaries parallel to the z-axis, τ_w is the shear stress, ρ is density of air, and λ is the distance measured normal from the nearest wall.

The shear stress at the limit of the near-wall region is assumed to be identical with that at the wall and it is approximated as following:

$$\tau_w = \mu\left(\frac{\partial u_i}{\partial \lambda}\right) \approx \mu\left(\frac{\Delta u_i}{\lambda}\right) = \mu\left(\frac{u_{i,\lambda} - u_{i,wall}}{\lambda}\right) = \mu\left(\frac{u_{i,\lambda}}{\lambda}\right) \tag{30}$$

where μ is the dynamic viscosity.

The near-wall value of turbulent kinetic energy (k) is calculated from the relationship:

$$k = \frac{|\tau_w|}{A_2^{1/2}\rho} \tag{31}$$

Experiments

Figure 2 shows the experimental setup. The push-pull system consisted of a 0.488cm x 0.488cm (0.192in x 0.192in) square jet with 61.0cm (24in) flange and a 8.99cm x 8.99cm (3.54in x 3.54in) square hood with 61.0cm (24in) flange. The distance between the jet and the hood was 40.6cm (16in). This push-pull system was placed in a 1.52m x 1.52m x 2.13m (5ft x 5ft x7ft) wind tunnel and the hood flow rate was set approximately to 14.2m³/min (500cfm). The jet flow rate was 0.0496m³/min (1.75cfm). For the push-pull with cross draft, cross flow velocities were set to 30.5m/min (100fpm) and 76.2m/min (250fpm) in the perpendicular direction to the coaxial line of the jet and hood.

A series of points was selected for velocity and turbulence kinetic energy measurements. Figure 3 displays these points on the plane ADJH of the Figure 1. The average velocity and turbulence fields are two-dimensional on this plane.

A smoke wire technique was used for flow visualization. This visualization technique is described in Appendix. Photographs and videos of the flow field were obtained to show the direction of velocity field. Velocity and turbulence fields were measured with a 1053B Thermo System Inc. (TSI) constant temperature anemometer. A probe supporter was positioned in a traversing unit to move the probe to the desired positions. The velocities were measured in correct direction using information from the visualization. Appendix describes calibration and measurement methods and the discussion of the limitations of the measurements.
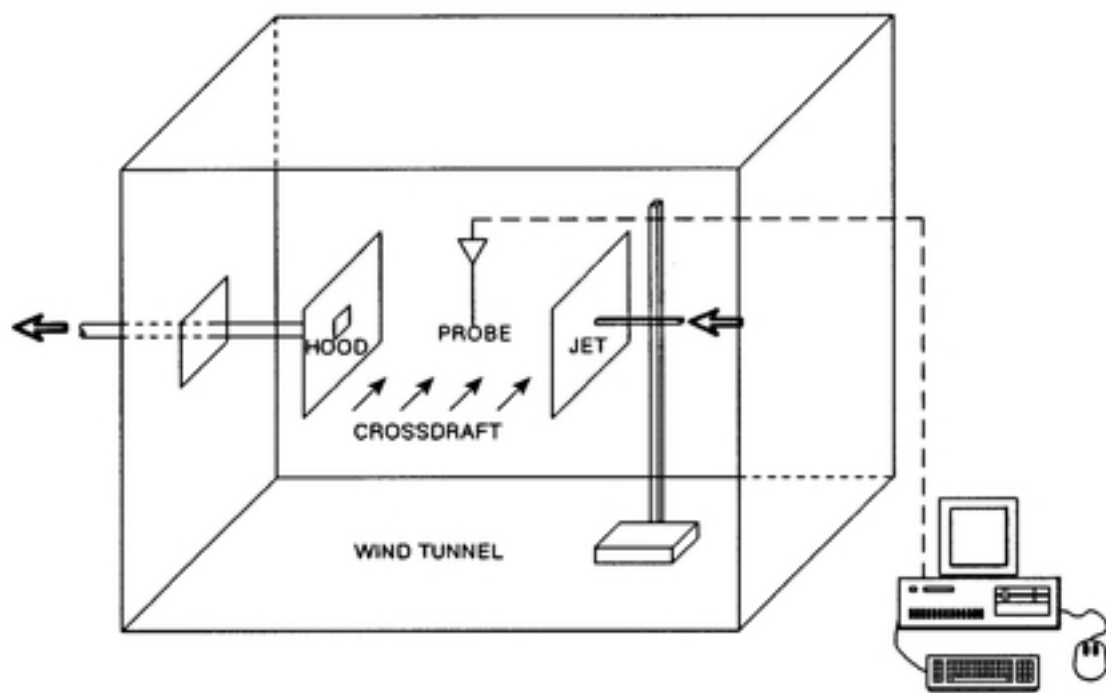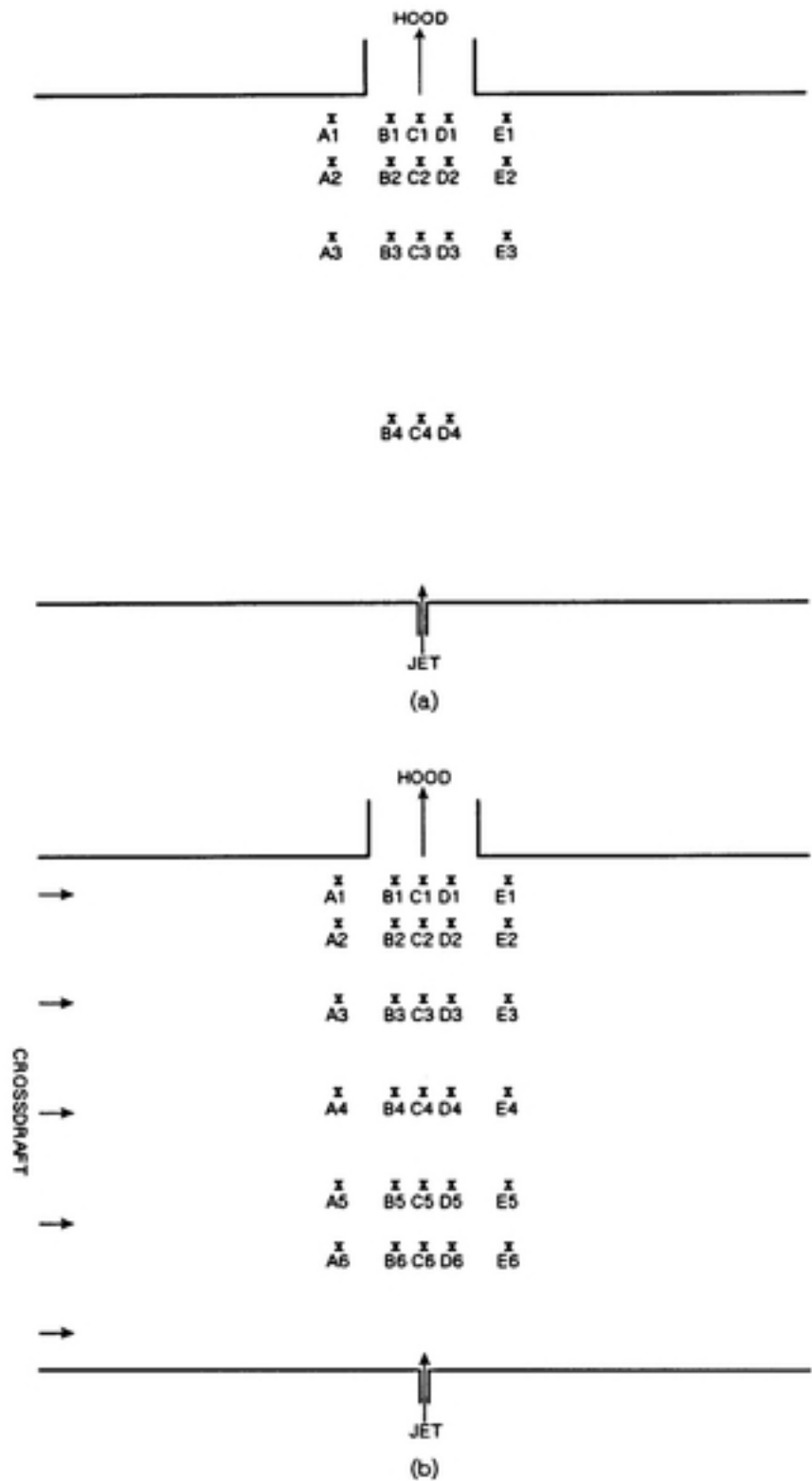
Figure 2. Experimental Set-Up

13

Figure 3. Measurement Points (a) The Push-Pull without Cross Draft (b) The Push-Pull with Cross Draft

Results

A Square Jet

A square jet flow was simulated as a preliminary test. Figure 4 shows a comparison of the predicted centerline velocities with the empirical reference data[20]. All distances were made dimensionless by dividing by one-half the width of the square jet (S) and all velocities were normalized with respect to the jet face velocity. The centerline velocities were predicted fairly well with little deviation in the vicinity of the jet in the far field. Figure 5 shows the turbulent kinetic energy distributions on the centerline. Only the values at far field were compared due to the lack of reference data near a jet. The prediction matched up well with the empirical data[21] at far field.

Figure 6 is the vector plot of the predicted velocity field of a square jet with cross flow. It shows bending of jet and reversed flow immediately behind the jet, which is consistent with the references[22-24]. Even though the degree of the bending of jet is less than that of Sykes et al.[22], there is strong resemblance between the reference figure and Figure 6. The discrepancy is considered partially due to the jet core boundary condition that keeps the jet straight on centerline in the jet core zone. The main reason may be the coarse grid system which prevented accurate calculation. The number of grid points was 25 x 12 x 17, which is far less than that of Sykes et al.[22] — 66 x 35 x 50.

A Square Jet and Square Hood without Cross Draft

A push-pull with a 0.192 in x 0.192 in square jet and a 3.54 in x 3.54 in square hood was simulated. The jet exit velocity was 6800 fpm and the hood face velocity (w_{ex}) was 5100 fpm. The grid system consists 14 x 14 x 20 nodes. Figure 7 shows the convergence histories for velocity and turbulent kinetic energy. Figure 8 is the predicted velocity field

15
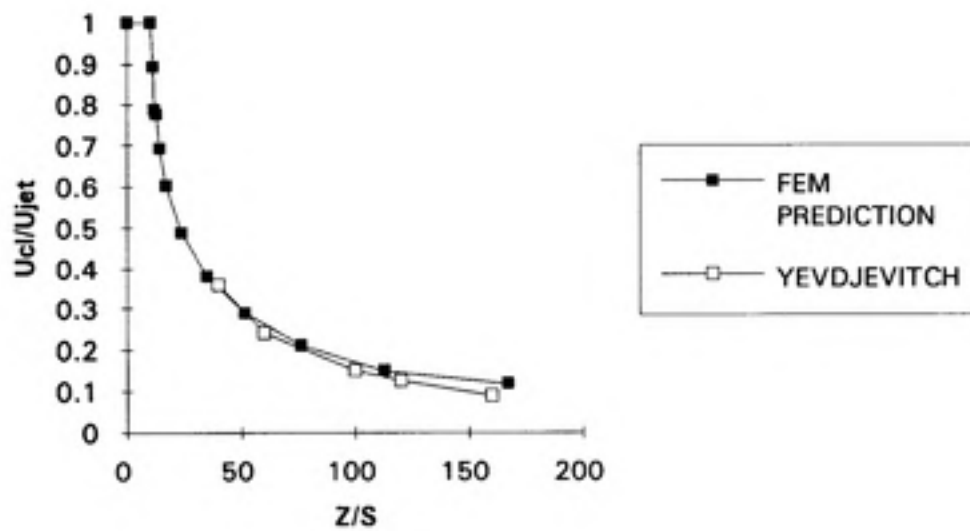
Figure 4. Centerline Velocity of the Square Jet. FEM PREDICTION is the prediction by the finite element method, and YEVDJEVITCH is the empirical data from the reference (20).
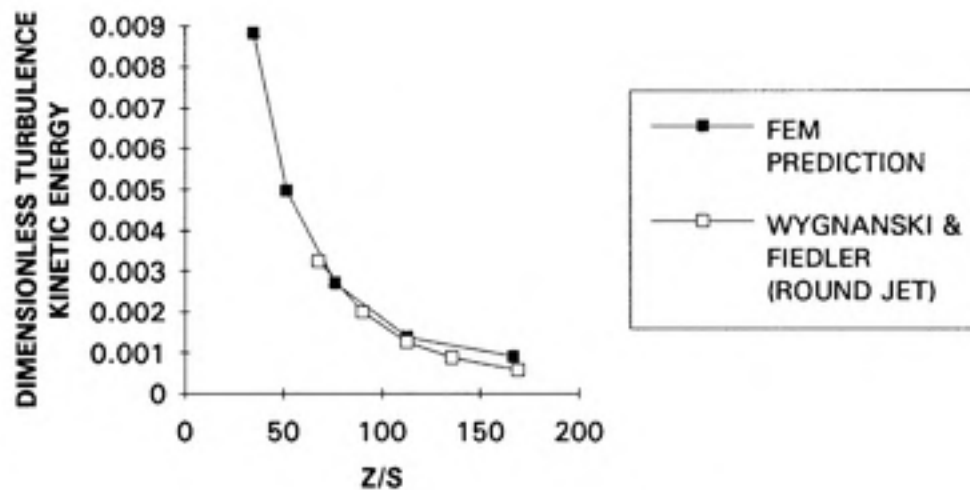

Figure 5. Turbulent Kinetic Energy on the Centerline of the Square Jet. FEM PREDICTION is the prediction by the finite element method, and WYGNANSKI & FIEDLER (ROUND JET) is the empirical data from the reference (21).
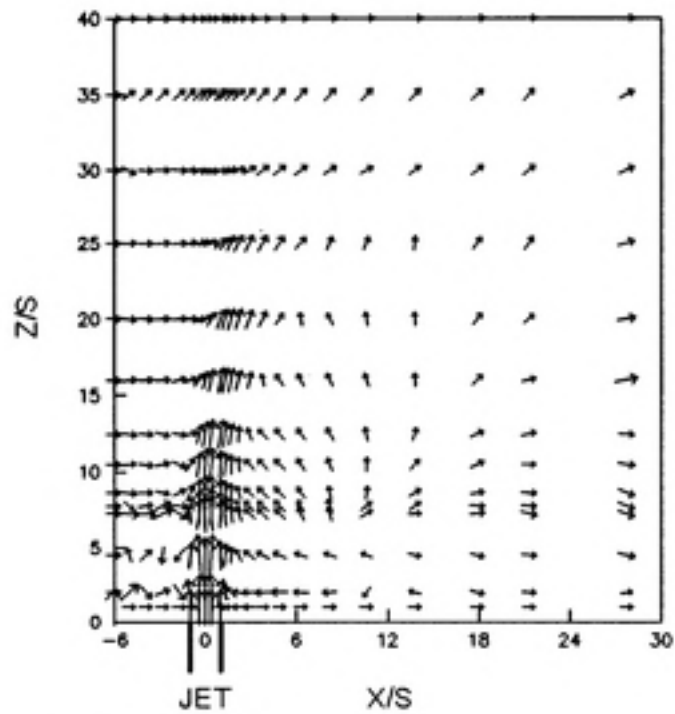
Figure 6. Predicted Velocity Vector Plot of the Square Jet into Cross Draft
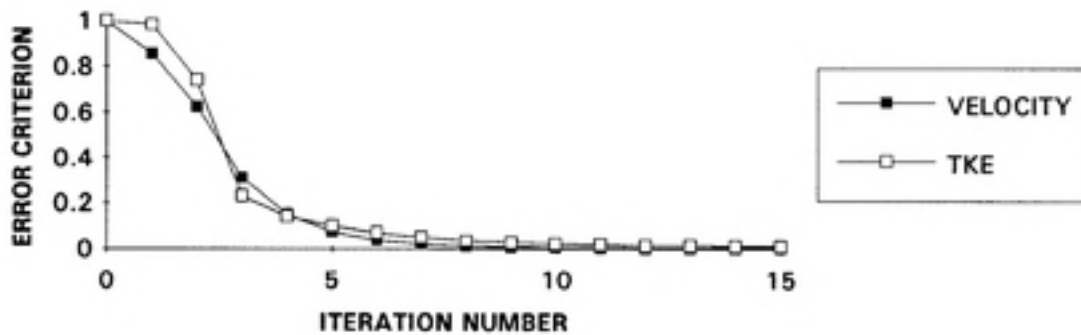
Figure 7. Convergence History of the Simulation of the Push-Pull without Cross Draft

17
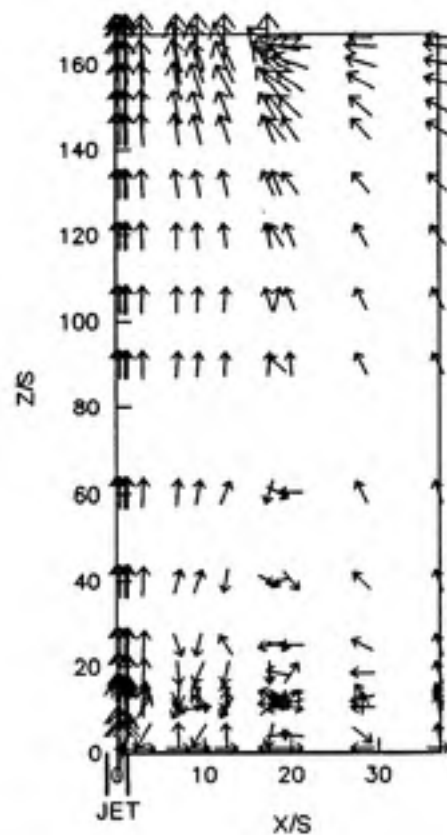
Figure 8. Predicted Velocity Vector Plot of the Push-Pull without Cross Draft

on the plane ADJH in the Figure 1. Figures 9 - 11 show the comparisons between the predictions and the measurement data. The least-squares linear-regression regression was performed between these values. The regression model is:

$$Y = SX + I \qquad (32)$$

where Y is the predicted value, X is the measured value, S and I are the slope and intercept of the regression line.

If the prediction perfectly matches the measurement, S should be 1.0 and I should be 0. The transformation to logarithms was used for the total velocity and turbulent kinetic energy values to compare data relatively and prevent deviations at lower values from being masked by larger deviations at higher values. Here Y is the log of the predicted values and X is the log of measured values. The statistical data given in Table 1. The parameter estimations are given together with the 95% confidence interval (CI) and the R^2

18
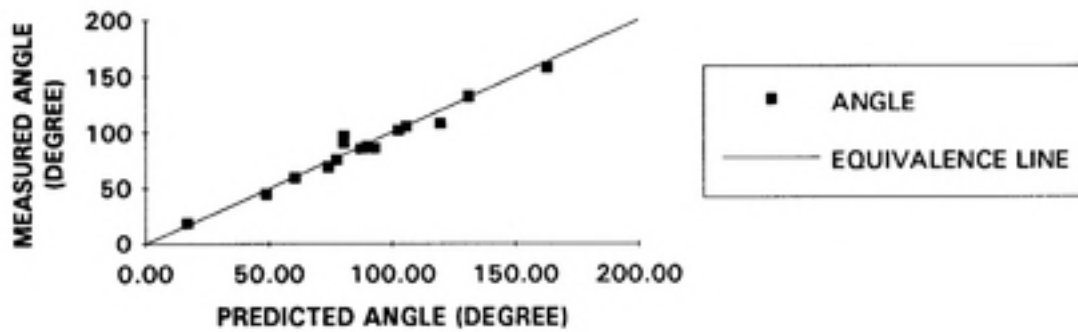
Figure 9. Velocity Angle of the Push-Pull without Cross Draft. Velocity angle is defined as 0 degree for the (+) x-axis and measured counterclockwise.
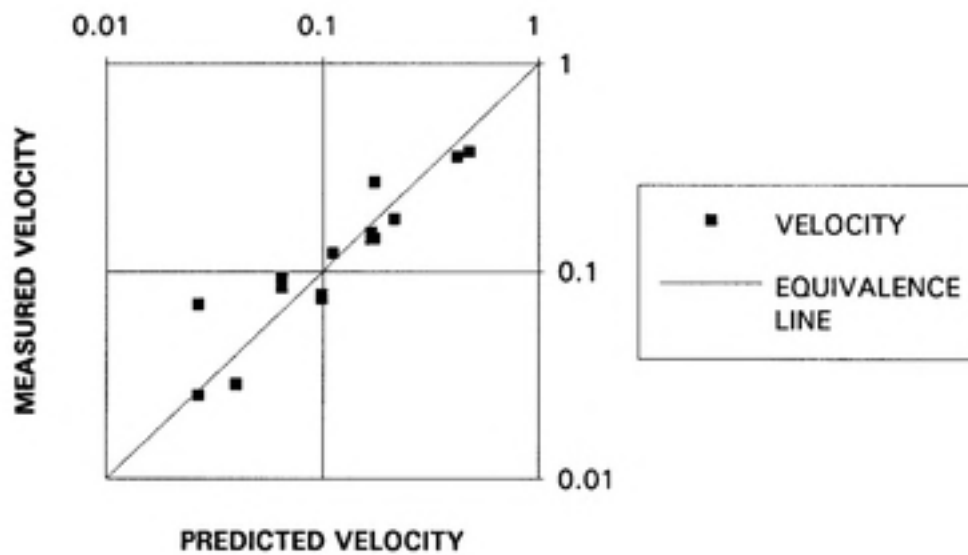
Figure 10. Total Velocity Magnitude of the Push-Pull without Cross Draft
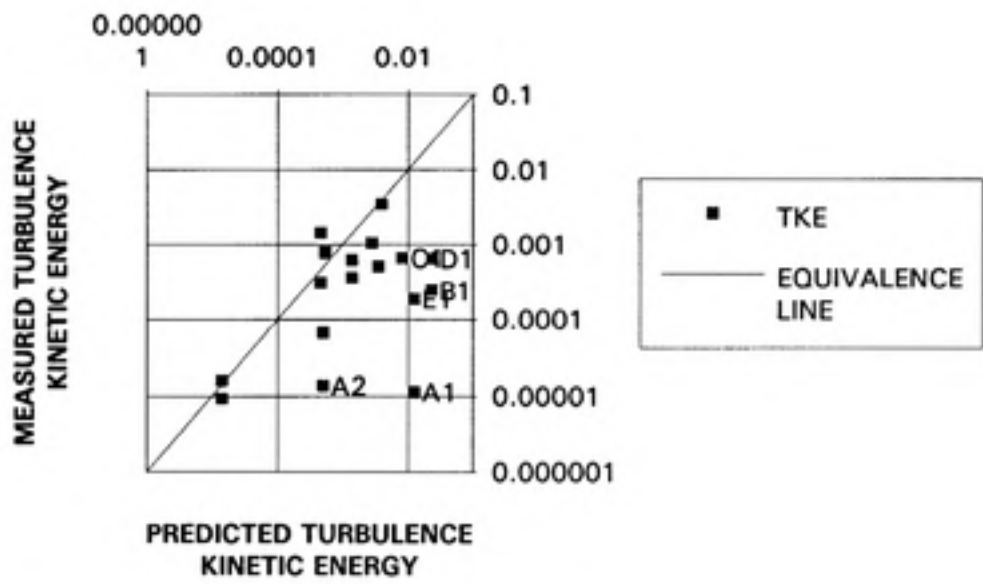
Figure 11. Turbulence Kinetic Energy of the Push-Pull without Cross Draft

Table 1. Regression Analysis for Predictions vs. Measurements
of the Square Jet and Square Hood without Cross Draft

Variable	Intercept (95% CI)	Slope (95% CI)	R^2 Values
Total Velocity	0.0132	0.9991	0.8626
	(-0.201, 0.2276)	(0.7877, 1.2104)	
Velocity Angle	0.3324	1.0102	0.9608
	(-9.682, 10.346)	(0.902, 1.1184)	
TKE	-1.012	0.512	0.1864
	(-3.121, 1.0965)	(-0.055, 1.079)	

values.

The 95% confidence intervals both for the intercepts and for the slopes include 0 and 1 in each case. The R^2 values are fairly high for velocity magnitude and velocity angle. However, R^2 for turbulence kinetic energy is low which indicates that the velocity prediction was good but turbulence was over-predicted in the vicinity of the hood. Turbulence kinetic energy prediction was reasonable except at the points in the vicinity of the hood (A1, A2, B1, C1, D1, E1 in the Figure 3 (a)).

A Square Jet and Square Hood with Cross Draft

Jet exit velocity was 6836 fpm at the jet face and the hood face velocity (w_{ex}) was 5500 fpm. The cross draft velocity (U_c) was 100 fpm and 250 fpm. The grid system consists of 26 x 11 x 18 points.

Figures 12 (a) and 12 (b) show the convergence histories for velocity and turbulent kinetic energy. These paths converged after having some problems at iteration level #5. Figures 13 and 14 represent the flow fields by the predictions and the experiments, respectively. The photograph shows excellent agreement with the predicted vector plots. Figures 15, 16, and 17 compare the predictions with the measurements.

The same linear regression analysis was performed for the evaluation of the predictions. When the data at points D5, D6, E5, E6 were removed as outliers because the turbulence intensity was so high that the measurements were not reliable, then the regressions repeated. Further explanations of restrictions of the measurement method in high turbulent regions are provided in Appendix.

Table 2 and Table 3 list the statistical data of the regressions. The 95% confidence intervals include 0 and 1 both for the intercepts and for the slopes in each case except one case (TKE with 100 fpm cross draft). Velocity predictions were reasonable but turbulence ones were not. There are significant discrepancies in near jet flow downstream where the

21

(a)

(b)
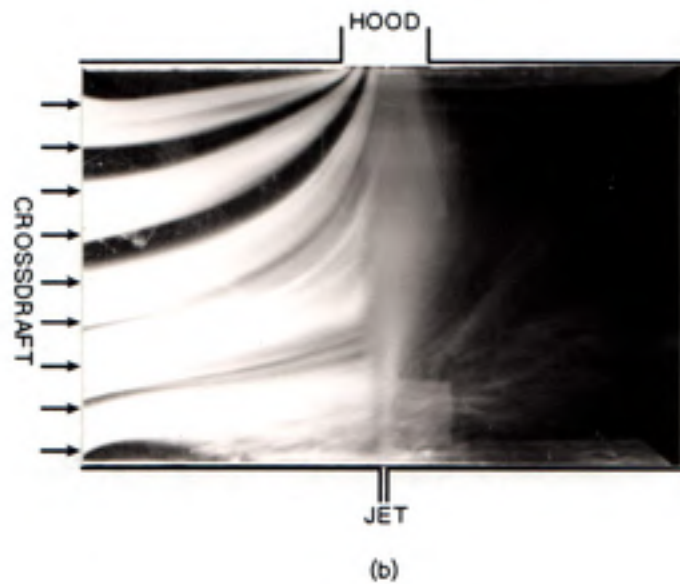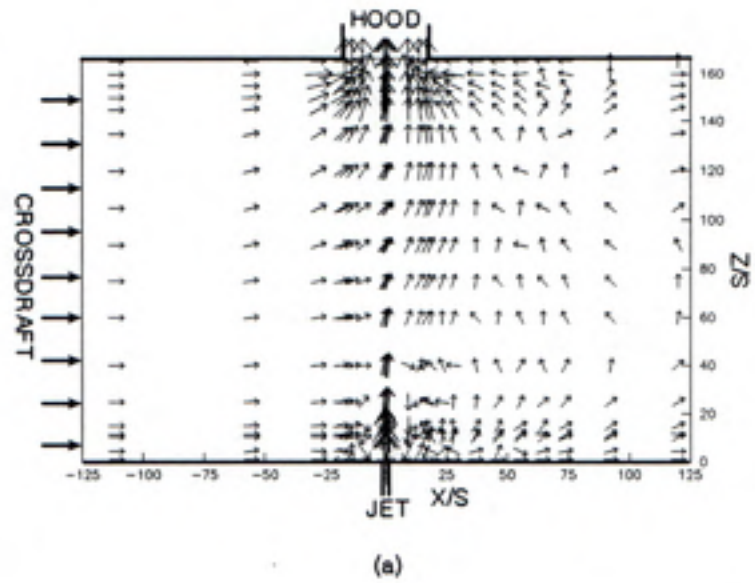
Figure 13. Velocity Field of the Push-Pull with Cross Draft 100 fpm
(a) Predicted Vector Plot (b) Flow Visualization

23
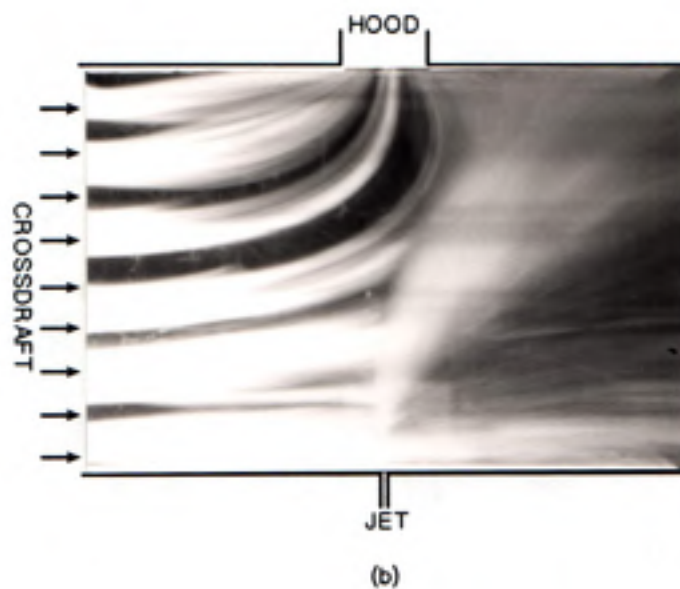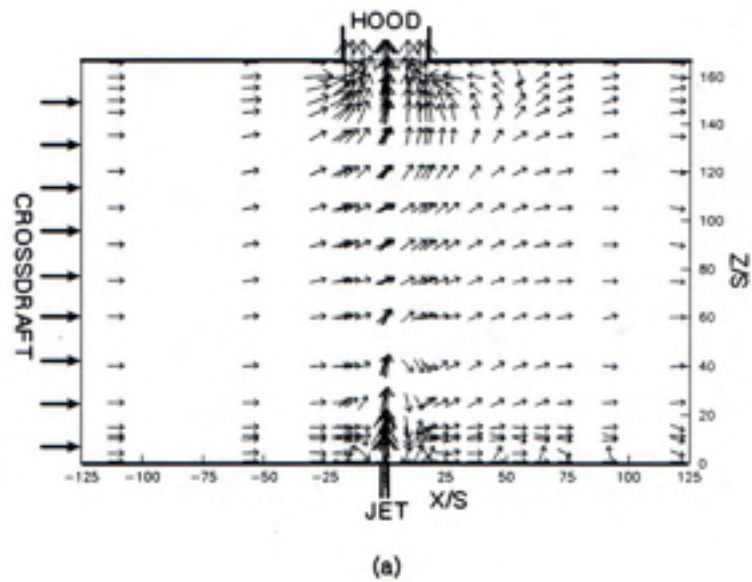
Figure 14. Velocity Field of the Push-Pull with Cross Draft 250 fpm
(a) Predicted Vector Plot (b) Flow Visualization

24
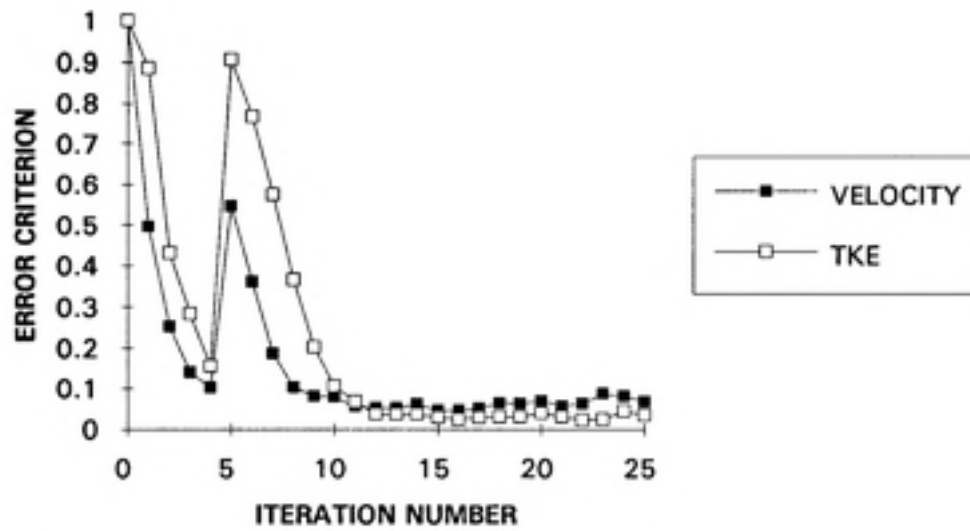
Figure 12 (a). Convergence History of the Simulation of the Push-Pull with Cross Draft 100 fpm
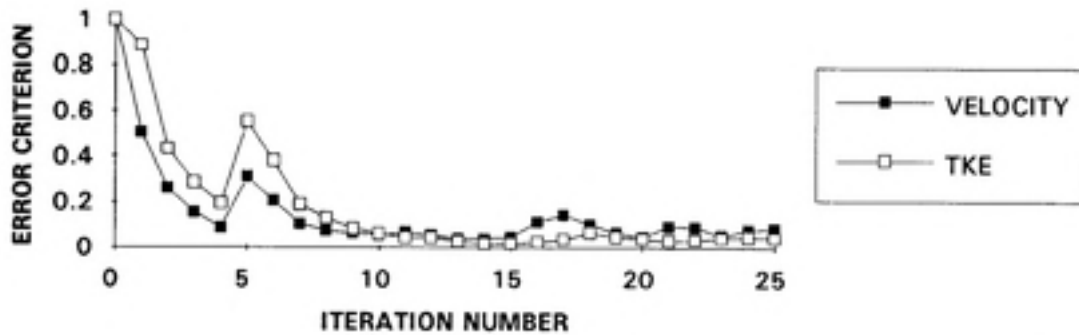
Figure 12 (b). Convergence History of the Simulation of the Push-Pull with Cross Draft 250 fpm
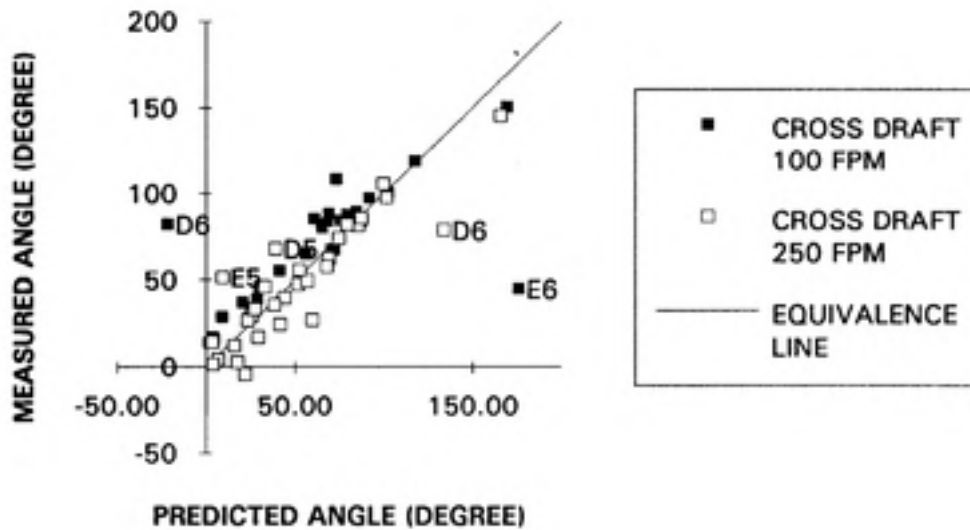
Figure 15. Velocity Angle of the Push-Pull with Cross Draft. Velocity angle is defined as 0 degree for the (+) x-axis and measured counterclockwise.
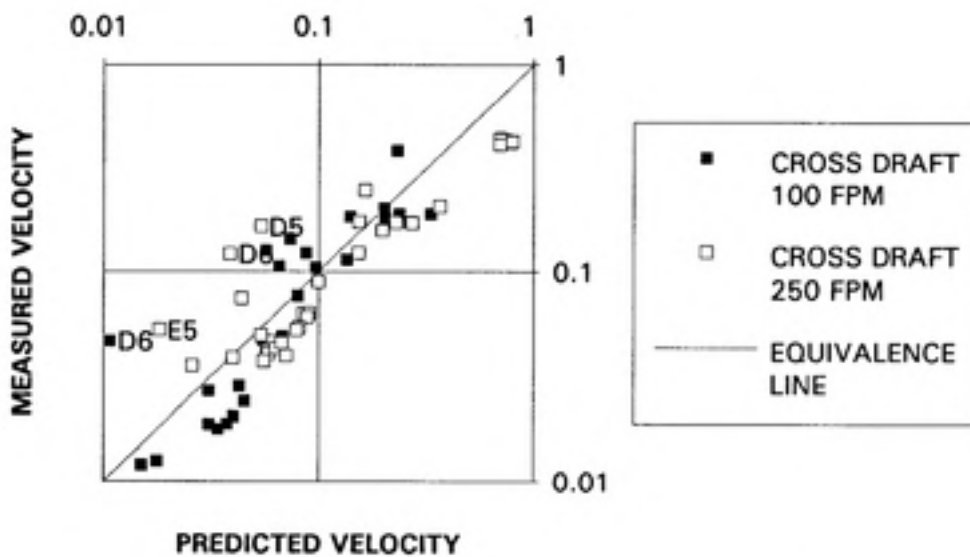
Figure 16. Total Velocity Magnitude of the Push-Pull with Cross Draft
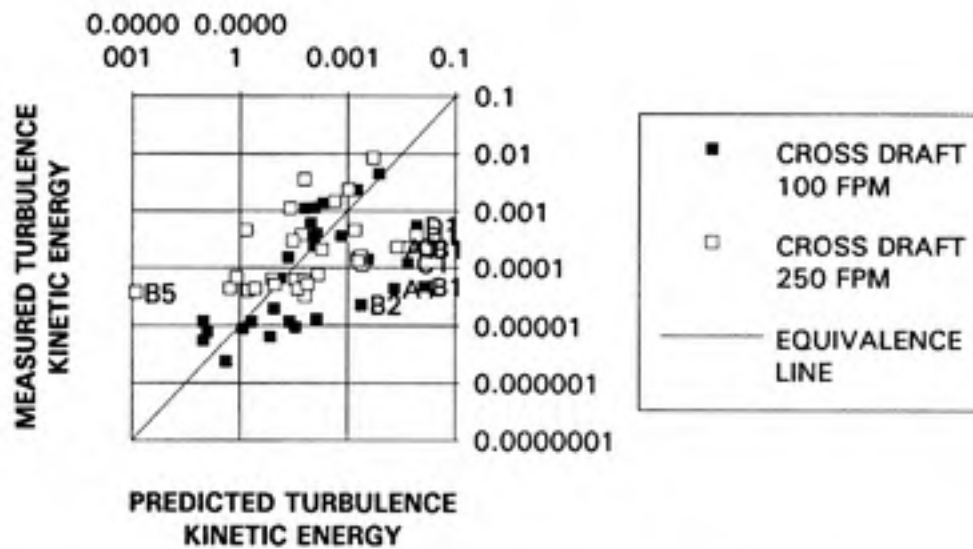
Figure 17. Turbulence Kinetic Energy of the Push-Pull with Cross Draft

Table 2. Regression Analysis for Predictions vs. Measurements
of the Square Jet and Square Hood with Cross Draft 100 fpm

Variable	Intercept (95% CI)	Slope (95% CI)	R^2 Values
Total Velocity	-0.0577 (-0.2667, 0.1513)	0.8980 (0.7250, 1.0710)	0.8015
Total Velocity (Without D6, E6)	-0.0691 (-0.2426, 0.1045)	0.8623 (0.7139, 1.0107)	0.8458
Velocity Angle	-3.6148 (-34.065, 26.835)	0.9480 (0.5546, 1.3414)	0.4653
Velocity Angle (Without D6, E6)	-16.177 (-25.736, -6.615)	1.1039 (0.9816, 1.2263)	0.9297
TKE	-0.6847 (-2.3570, 0.9876)	0.7275 (0.3281, 1.1269)	0.3321
TKE (Without the 5 Points)	-1.0773 (-2.116, -0.0388)	0.7020 (0.4527, 0.9514)	0.6078

Table 3. Regression Analysis for Predictions vs. Measurements
of the Square Jet and Square Hood with Cross Draft 250 fpm

Variable	Intercept (95% CI)	Slope (95% CI)	R^2 Values
Total Velocity	0.0132 (-0.201, 0.2276)	0.9991 (0.7877, 1.2104)	0.8626
Total Velocity (Without D5, D6, E5)	0.1597 (-0.0039, 0.3232)	1.0459 (0.8993, 1.1926)	0.8962
Velocity Angle	4.2631 (-7.167, 15.694)	0.9949 (0.8023, 1.1874)	0.8000
Velocity Angle (Without D5, D6, E5)	6.2163 (-0.7760, 13.209)	0.9744 (0.8548, 1.0939)	0.9185
TKE	-0.7181 (-3.119, 1.6758)	0.7830 (0.1519, 1.4141)	0.1874
TKE (Without the 5 Points)	-1.3511 (-3.331, 0.6288)	0.6855 (0.1676, 1.2034)	0.2372

high velocity flow mixes with entraining flow and the measurement data were not accurate. This region is not our major concern, which is at near the hood. The prediction of velocity field is reasonable at other points. Turbulence predictions are not very good as in the case without cross draft. It is over-predicted in the vicinity of the hood. The points of over-prediction are shown in the Figure 17 (A1, B1, B2, C1, D1 in the Figure 3 (b)). Generally, more over-predictions were observed in lower cross flow (100 fpm) case. It still shows some linear relationship against the measurements if the over-predictions near the hood are ignored.

Discussion

The discrepancy of the turbulence kinetic energy at the near-hood points is considered due to the simple one-equation turbulence model and numerical errors caused by calculations on coarse grid.

The calculations on the coarse grid prevent accurate calculations in the convection-dominated region. The grid system was coarse because the three-dimensional problem produced a huge global matrix, which needs large computer memory and prevents calculation on finer grids. The size of matrix can be greatly reduced by replacing the direct solver with an iterative method. However the penalty terms were calculated with reduced numerical integration and the penalty method produces ill-conditioned matrix, which causes slow convergence for iterative solvers. The use of the penalty-FEM with iterative solvers has been limited due to this convergence problem. A recent study[25] reported that iterative solvers of conjugate gradient method incorporated successfully for the penalty-finite element method.

This study used a simple one-equation turbulence model with arithmetic expression for the length scale, which was empirically determined to fit the straight jet and then was applied successfully to a jet into cross draft[11]. However, it is difficult to specify the length scale distribution for the flow of the push-pull. Viscous effect dominates over turbulence in the vicinity of the hood. The length scale does not reflect the effect of hood addition.

The flow visualization and the turbulence measurements showed that viscous effects dominate turbulence in the vicinity of the hood. Based on this fact, both the length scale and the turbulence kinetic energy values should be very small and the following modification is proposed to adjust the original length scale:

$$\Lambda' = \Lambda(1 - \exp(-cR)) \tag{33}$$

28

$$R = \frac{k^{1/2}d}{v} \qquad (34)$$

$$d = 0.025r_h \qquad (35)$$

where Λ' is the modified length scale, c is a model constant, R is the ratio of turbulence force to viscous force, d is the length scale inferred from the equation (5)[11], and r_h is the distance from the center of the hood.

This modified length scale is to include viscous effects by the presence of the hood. The value of modified length scale become smaller, as the distance from the hood is shorter and as turbulence value is smaller. Thus it will lessen the over predictions near the hood. However, this length scale can not incorporate non-axisymmetric effects by cross draft. Two-equation models account not only for the transport of the turbulence velocity scale but also that of the length scale. Therefore, two-equation models are used widely for flows for which the length-scale cannot be described empirically in an easy way[26] Two-equation models are known to be more general and robust for turbulence problems and the k-ε models have been widely used to solve turbulent flows problems. However they increase the size of problem and computational efforts, which is critical in this kind of large size problem.

The over-prediction of turbulence may not influence much in predicting the concentration field because convection dominates over diffusion at the near-hood region.

Conclusions

Push-pull ventilation is an attempt to improve local exhaust ventilation. Numerical modeling is an effective tool in ventilation design. The complex characteristics of the flow in the push-pull system causes difficulties in finding a proper turbulence model and in employing effective numerical calculations.

A three-dimensional finite element model was used to simulate push-pull ventilation which consists of a square jet and a square hood. Disruption of the flow was simulated by employing cross draft. Velocity and turbulence fields were measured using a smoke technique and a hot-film anemometry.

Velocity predictions were reasonable in all simulations tested. Turbulence predictions were not good at the points near the hood where viscous effects dominates turbulence. There were limitations of the simple turbulence model and the direct solver. Iterative solvers and better turbulence models are to be used in future studies.

References

(1) American Conference of Governmental Industrial Hygienists, *Industrial Ventilation - A Manual for Recommended Practice*, 21st edition, ACGIH, Cincinnati, OH, 1992.

(2) Hampl, V. and Hughes, R. T., Improved Local Exhaust Control by Directed Push-Pull Ventilation System., *Am. Ind. Hyg. Assoc. J.*, 47(1):59-65 (1986).

(3) Heinsohn, R. J., *Industrial Ventilation: Engineering Principles*, John Wiley & Sons, Inc., New York (1991).

(4) Heinsohn, R. J. et al., Viscous Turbulent Flow in Push-Pull Ventilation Systems., *Ventilation '85*, Elsevier Science, New York (1986).

(5) Lage, J. L. et al. Efficiency of Transient Contaminant Removal from a Slot Ventilated Enclosure., *Int. J. Heat Mass Transfer.*, 2603-2614 (1991).

(6) Patankar, S. V., *Numerical Heat Transfer and Fluid Flow*, Hemisphere, New York (1980).

(7) Launder, B. E. and Spalding, D. B., The Numerical Computation of Turbulent Flows., *Comput. Mthds. Appl. Mech. and Engnr.*, 3:269-289 (1974).

(8) Damin, Z. et al., Numerical Solutions of Navier-Stokes Equation for Push-Pull Flow., *ASHRAE Trnas.*, 95(2):23-29 (1989).

(9) Kurabuchi, T., Kato, S., and Kamata, M., Numerical Study on Three-Dimensional Turbulent Flow with Inflow and Outflow Boundary Condition given in Static Pressure., *Journal of the Faculty of Engineering, the University of Tokyo*, Series A, 20:8-9 (1982).

(10) Flynn, M. R., *Final Report: NIOSH Grant 5 R01 OH02710-01(2)* (1993).

(11) Sykes, R. I. et al., On the Vorticity Dynamics of a Turbulent Jet in a Cross flow., *J. Fluid Mech.*, 168:393-413 (1986).

(12) Huyakorn, P. S., and Pinder, P. S., *Computational Methods in Subsurface Flow*, Academic Press, Inc., San Diego, CA, 1983.

31

(13) Press, W. H., et al., *Numerical Recipes - The Art of Scientific Computing*, Cambridge University Press, New York, NY, 1986.

(14) Hughes, T. J. R. et al., A. Finite Element Analysis of Incompressible Viscous Flows by the Penalty Formulation., *J. Coumpt. Phys.*, 30:1-60 (1979).

(15) Reddy, J. N., On Penalty Function Methods in the Finite Element Analysis of Flow Problems., *Int. J. Numer. Mthds. Fluids*, 2:151-171 (1982).

(16) Hughes, T. J. R., A Simple Scheme for Developing 'Upwind' finite Elements., *Int. J. Numer. Mthds. in Engnr.*, 12:25-42 (1982).

(17) Thomas, C. E. et al., A Finite Element Analysis of Flow Over a Backward Facing Step., *Computers and Fluids*, 9:265-278 (1981).

(18) Thomas, C. E. et al., Modeling Flow over a Backward-Facing Step Using the F.E.M. and the Two-Equation Model of Turbulence., *Int. J. numer. Mthds. in Fluids*, 1:295-304 (1981).

(19) Caille, J. and Schets, J. A., New Wall Treatment for Numerical Navier-Stokes Solution of Incompressible Turbulent Flows., *AIAA Journal*, 31(1):20-26 (1993).

(20) Yevdjevitch, V. L., Diffusion of Slot Jets with Finite Orifice Length-Width Ratios., *Hydraulics Papers*, Colorado State University, Fort Collins (1966).

(21) Wygnanski, I. and Fiedler, H., Some Measurements in the Self-Preserving Jet., *J. Fluid Mech.*, 38(3):577-612 (1969).

(22) Sykes, R. I. et al., On the Vorticity Dynamics of a Turbulent Jet in a Cross flow., *J. Fluid Mech.*, 168:393-413 (1986).

(23) Rudinger, G. and Moon, L. F., Laser-Doppler Measurements in a Subsonic Jet Injected Into a Subsonic Cross Flow., *Journal of Fluids Engineering*, Trans. ASME., 516-522 (1976).

(24) Patankar, S. V., Prediction of the Three-Dimensional Velocity Field of a Deflected Turbulent Jet., *Journal of Fluids Engineering*, Trans. ASME., 758-762 (1977).

(25) Reddy, M. P., Penalty-Finite Element Analysis of Incompressible Flows Using Element-by-Element Solution Algorithms., *Comput. Mthds. Appl. Mech. and Engnr.*, 100(2):169-205 (1992).

(26) Rodi, W., *Turbulence Models and Their Application in Hydraulics - A State of the Art Review*. (1984).

Appendix

Rotometer Calibration

Compressed air was released from a laboratory compressed air tank. The air was regulated to the pressure of 28 lb/in² by a Matheson pressure regulator and then supplied to a Dwyer rotometer with 0-100 ft³/hour (cfh) measurement range. The rotometer was calibrated with an American Meter Company wet test meter with maximum capacity of 240 cfh. The data for the calibration are presented in Table A1. The linear regression line for the data is:

$$W = -12.07 + 1.205\ R \quad (\ r^2 = 0.999\ ) \tag{A1}$$

where W is the wet test meter reading in cfh, and R is the rotometer reading in cfh.

Table A1. Rotometer Calibration Data

Rotometer Reading (cfh)	Wet Test Meter Reading (cfh)
60	60.1
65	66.9
70	71.9
75	78.0
80	84.3
85	90.9
90	96.2
95	101.9
100	108.9

Orifice Calibration

Orifice calibration was performed using the pitot traverse method with a Dwyer pitot tube and a Dwyer microtector. The microtector is specified to be accurate and repeatable to ± 0.00025 inches water column ("H_2O). A sharp edged orifice, 8 inches in diameter, was mounted in a 12 inches diameter duct. The orifice meter was calibrated by using 10 points pitot traverses in a 6 inches diameter duct. The data for the calibration are given in Table A2. The linear regression line for the data is:

$$Q = 31.70 + 937.6 \sqrt{h} \ (r^2 = 0.999) \tag{A2}$$

where Q is the calibration flow in ft³/min (cfm), and h is the orifice meter pressure drop in "H_2O.

Hot Film Sensor Calibration

Velocities were measured with a 1053B Thermo system Inc. (TSI) constant

Table A2. Orifice Meter Calibration Data

[Orifice Meter Pressure Drop ("H_2O)]$^{0.5}$	Calibration Flow (cfm)
0.20	214
0.30	314
0.40	403
0.50	512
0.54	535
0.60	605
0.70	677
0.80	785
0.89	877
0.99	948

temperature anemometer. A 1240-20 TSI Platinum hot film sensor of the "X" configuration was mounted on a 1155-18 TSI dual sensor probe support. The support was attached to an angle measurement system, which has accuracy of ±0.25°. The sensors were calibrated in the orientation of 45° to the calibrating flow. Calibrations was performed in two different ways. Low velocity calibration was executed in a low velocity wind tunnel. The sensors were positioned at the center of the wind tunnel and the bridge voltages of both sensors were collected for a range of velocities determined by orifice meter readings. High velocity calibration was achieved in a specially designed wind tunnel. A 3 inches diameter Plexiglas duct with a trombone bell mouse was fitted with plastic straws and fine mesh screen so that they could suppress turbulence level. The probe was positioned downstream of the honeycombs and the bridge voltages were recorded for a range of velocities, which were measured directly using a pitot tube at the same position as that of the probe. The data for the calibration are presented in Table A3. The linear regression lines for the data are:

Velocity Range : 47 - 360 fpm

$$\text{Sensor \#1} \quad [Vel]^{0.5} = -14.667 + 2.4216 \, [Volt \, 1]^2 \, (r^2 = 0.998) \tag{A3}$$

$$\text{Sensor \#2} \quad [Vel]^{0.5} = -13.860 + 2.3803 \, [Volt \, 2]^2 \, (r^2 = 0.999) \tag{A4}$$

where Vel is the velocity normal to the sensor in fpm, $Volt \, 1$ is the #1 sensor bridge voltage in volts, and $Volt \, 2$ is the #2 sensor bridge voltage in volts.

Velocity Range : 360 - 4200

$$\text{Sensor \#1} \quad [Vel]^{0.5} = -17.709 + 2.6737 \, [Volt \, 1]^2 \, (r^2 = 0.999) \tag{A5}$$

$$\text{Sensor \#2} \quad [Vel]^{0.5} = -18.928 + 2.8132 \, [Volt \, 2]^2 \, (r^2 = 0.999) \tag{A6}$$

Wind Tunnel Calibration

A fan for the wind tunnel was controlled with a Toshiba Tosvert-130H1 transistor inverter. Velocities in the wind tunnel were calibrated against varying frequencies of the

Table A3. Hot Film X-Probe Calibration Data

[Velocity Normal to the Sensor (fpm)]$^{0.5}$	[#1 Sensor Bridge Voltage (Volt)]^2	[#2 Sensor Bridge Voltage (Volt)]^2
6.820	8.773	8.675
8.482	9.532	9.413
9.632	10.11	9.831
11.34	10.82	10.58
13.11	11.52	11.41
14.74	12.19	11.99
16.56	12.80	12.74
18.33	13.60	13.54
19.27	13.49	13.36
21.45	14.55	14.39
26.14	16.49	16.12
28.58	17.50	17.04
31.57	18.51	18.02
35.67	20.24	19.37
40.21	21.76	21.03
43.61	23.03	22.21
48.66	24.70	24.03
53.13	26.31	25.63
56.73	27.75	26.78
62.40	30.01	28.72
64.66	30.76	29.91

inverter. The velocities were measured at the 9 points representing 9 partisans the plane of experimental measurement. The data for the calibration are presented in Table A4. The linear regression line for the data is:

$$V = -21.335 + 7.6433\, F\ (\ r^2 = 0.999\ ) \tag{A7}$$

where V is the wind tunnel velocity in fpm, and F is the frequency of the inverter.

The spatial variation of the velocities was 4~16% for the range of calibration velocities. There was also the angle deviation of -2°~7° from the perpendicular direction to the wind tunnel face. The most variation and deviation occurred at the lowest velocity.

Flow Visualization

Flow field could be visualized with a smoke wire technique smoke generation technique is used in order to visualize air flow. Several wires were twisted together and stretched perpendicularly to the direction of cross flow. Paraffin oil was coated on the wires and then direct current was connected through a Variable Auto-transformer so that dense smoke generated. The flow was illuminated by an ILC arc lamp modulator. Flow field scenes were recorded by a video cassette recorder and velocity direction at the measurement points were roughly estimated from the scenes. This information was used later on measuring of velocity field with the anemometer. Top view photographs were taken through a transparent window at the top of the wind tunnel.

Table A4. Wind Tunnel Calibration Data

Inverter Frequency	Wind Tunnel Velocity (fpm)
15	85.4
20	134.1
25	176.0
30	212.9
35	245.1
40	282.4
45	319.1
50	361.6

38

Velocities were measured with the 1053B Thermo system Inc. (TSI) constant temperature anemometer. The calibrated "X" hot film sensors was mounted on the sensor probe support. The support was connected to the angle measurement mechanism which is scaled to 0.5° and has reading accuracy of ±0.25°. Analog outputs from the anemometer were converted to digital data by a MetraByte DAS-20 A/D converter which has a 8.5 microsecond conversion rate. The data were stored in a personal computer and used for velocity and turbulence calculations. The probe support rotated 360° freely by a motor which was remote-controlled outside the wind tunnel.

The sensors were rotated until average values of velocity data for both the probes were almost equal. Thus the sensors were set in the orientation of 45° to the flow, which is the same way as the calibration procedure. The information from the smoke wire method was used for all measurements. The sampling rate of velocity was 20/sec and sampling time was 50 sec. Average turbulence intensities were acceptably consistent (within 5%) in 15 sec sampling time in all measurements.

The sensors were regularly cleaned with acetone. The probe calibration was performed at 22 °C. Bridge voltage corrections were made in order to account temperature change. Velocity and turbulence intensity calculations were performed under the assumptions that:

i) the average velocity component perpendicular to the measurement plane is zero.

ii) the velocity must be limited to a single quadrant.

iii) there is no heat transfer due to the flow parallel to the sensor.

iv) there is no support interference.

v) the component of velocity fluctuations perpendicular to the measurement plane is small.

The relative error in the measurement of mean velocity and turbulence is a function of the turbulence intensity. As turbulence intensity increases, error also increases. As a

turbulence intensity more than 30%, measurement accuracy is not reliable. The error due to ignoring v is about 8% when the turbulence intensity is 20% for isotropic, normally distributed, and normally correlated turbulence.

The traversing unit was handled outside the wind tunnel in which the push-pull system installed. Resetting the probe to a specific position for every measurement, velocity measurements were repeated 5 times in an attempt to assess errors resulting from probe positioning. The velocities were within ±1% of the average value.

The jet and hood aligned to have common centerline on the measurement plane. The alignment was achieved by using a telescope tubing, the moving mechanism, scales. Bad alignment might cause considerable measurement errors, however these errors are hard to quantify. Two independent sets of measurements were made at same measurement points on the plane of push-pull in 250 fpm cross draft. Comparing the paired data of symmetric positions, the average velocity difference was 0.4% and the angle difference was ±10°. The average turbulence difference was 5%.

Velocities were measured at the hood face (actually, 3/8" from the exact hood face) in order to see if hood face velocity is uniform. Measurements were made at 7 points on the horizontal line connecting the half height of the hood. The velocity values were within ± 7% of the average value.

Hood flow rate was first set to 500 cfm with the calibrated orifice meter. The real duct work for the push-pull system was quite different from the straight one used for the orifice calibration. The flow rate was checked with pitot traverses in the real push-pull set up, resulted in 5% difference from the orifice meter reading.